

# Space Weather®



## RESEARCH ARTICLE

10.1029/2021SW002988

### Special Section:

Space Weather Impacts on  
Electrically Grounded Systems  
at Earth's Surface

### Key Points:

- 3D modeling of geomagnetically induced currents (GICs) is successfully validated against a field trial on a transmission line in southern Sweden
- Peak GIC during historical major geomagnetic disturbances exceed 100 A for one storm interval
- The peak GIC during the sudden impulse phase of a “perfect” storm exceeds 300~A

### Supporting Information:

Supporting Information may be found in the online version of this article.

### Correspondence to:

L. Rosenqvist,  
[lisa.rosenqvist@foi.se](mailto:lisa.rosenqvist@foi.se)

### Citation:

Rosenqvist, L., Fristedt, T., Dimmock, A. P., Davidsson, P., Fridström, R., Hall, J. O., et al. (2022). 3D modeling of geomagnetically induced currents in Sweden—validation and extreme event analysis. *Space Weather*, 20, e2021SW002988. <https://doi.org/10.1029/2021SW002988>

Received 25 NOV 2021

Accepted 16 FEB 2022

### Author Contributions:

**Investigation:** L. Rosenqvist, T. Fristedt, A. P. Dimmock, R. Fridström, L. Hesslow, M. Yu Smirnov, D. Welling, P. Wintoft

**Methodology:** L. Rosenqvist, P. Davidsson, J. O. Hall







**Validation:** L. Rosenqvist, T. Fristedt, R. Fridström, L. Hesslow

**Writing – original draft:** L. Rosenqvist

© 2022. The Authors.

This is an open access article under the terms of the [Creative Commons Attribution License](https://creativecommons.org/licenses/by/4.0/), which permits use, distribution and reproduction in any medium, provided the original work is properly cited.

## 3D Modeling of Geomagnetically Induced Currents in Sweden—Validation and Extreme Event Analysis

L. Rosenqvist<sup>1</sup> , T. Fristedt<sup>2</sup>, A. P. Dimmock<sup>3</sup> , P. Davidsson<sup>1</sup>, R. Fridström<sup>1</sup>, J. O. Hall<sup>1</sup>, L. Hesslow<sup>1</sup> , J. Kjäll<sup>1</sup>, M. Yu Smirnov<sup>4</sup> , D. Welling<sup>5</sup> , and P. Wintoft<sup>3</sup> 

<sup>1</sup>Swedish Defence Research Agency, Stockholm, Sweden, <sup>2</sup>Department of Marine Technology, Multiconsult Norge AS, Tromsø, Norway, <sup>3</sup>Swedish Institute of Space Physics, Uppsala, Sweden, <sup>4</sup>Luleå University of Technology, Luleå, Sweden, <sup>5</sup>University of Texas at Arlington, Arlington, TX, USA

**Abstract** Rosenqvist and Hall (2019), <https://agupubs.onlinelibrary.wiley.com/doi/abs/10.1029/2018SW002084> developed a proof-of-concept modeling capability that incorporates a detailed 3D structure of Earth's electrical conductivity in a geomagnetically induced current estimation procedure (GIC-SMAP). The model was verified based on GIC measurements in northern Sweden. The study showed that southern Sweden is exposed to stronger electric fields due to a combined effect of low crustal conductivity and the influence of the surrounding coast. This study aims at further verifying the model in this region. GIC measurements on a power line at the west coast of southern Sweden are utilized. The location of the transmission line was selected to include coast effects at the ocean-land interface to investigate the importance of using 3D induction modeling methods. The model is used to quantify the hazard of severe GICs in this particular transmission line by using historic recordings of strong geomagnetic disturbances. To quantify a worst-case scenario GICs are calculated from modeled magnetic disturbances by the Space Weather Modeling Framework based on estimates for an idealized extreme interplanetary coronal mass ejection. The observed and estimated GIC based on the 3D GIC-SMAP procedure in the transmission line in southern Sweden are in good agreement. In contrast, 1D methods underestimate GICs by about 50%. The estimated GICs in the studied transmission line exceed 100 A for one of 14 historical geomagnetic storm intervals. The peak GIC during the sudden impulse phase of a “perfect” storm exceeds 300 A but depends on the locality of the station as the interplanetary magnetic cloud hits Earth.

**Plain Language Summary** A dangerous consequence of extreme solar flares is a serious and prolonged disruption in the electricity supply. Society is now extremely dependent on electricity, so this raises numerous issues ranging from societal security to large economical losses. To avoid this, it is important to understand how strong the ground-induced currents (GICs) that arise as a consequence of the solar eruption can be, and which areas are vulnerable. GICs depend on how large and quickly the geomagnetic field at ground level changes and also the properties of the ground underneath. This study use a full 3D model to investigate the importance of lateral conductivity gradients at for example, coastal areas, on the severity of GICs in Sweden. The model is validated against a tailored field trial on a transmission line in a coastal area. Historical recordings of major storms is applied to the model in order to investigate how strong GICs can be expected in this particular transmission line. To understand a worst-case scenario, an ideal extreme solar storm and the simulated impacts in Sweden have been investigated.

## 1. Introduction

The fluctuating natural electric current system in the upper atmosphere poses operational threats to electric power transmission systems. The Sun occasionally releases violent eruptions that travel through interplanetary space and interact with Earth causing these current systems to be enhanced and exhibit rapid changes with time and space. These so-called geomagnetic storms and the associated geomagnetic disturbances (GMDs) cause, via electromagnetic induction, secondary induced electric currents to flow in the ground. The currents flow in both man-made current paths (such as telegraph systems, submarine cables, pipelines, and electric power grids) as well as in natural current paths following conducting structures in the ground and nearby water volumes. Due to the skin depth effect and the varying electrical conductivity structure of the Earth's subsurface the frequency content of the resulting so-called ground-induced currents (GICs) will be affected. GMDs typically last between several hours to several days resulting in a quasi DC current in the period range between seconds to several

#### Writing – review & editing:

L. Rosenqvist, T. Fristedt,  
A. P. Dimmock, P. Davidsson,  
R. Fridström, J. O. Hall, L. Hesslow,  
J. Kjäll, M. Yu Smirnov, P. Wintoft

thousand seconds to flow through power lines. Transformer groundings at power grid substations serve as entry points for GICs. These can cause transformer damage and voltage stability problems, which in turn can lead to partial or system-wide blackouts. Several such historical events have occurred. The first reported in 1940 after a strong geomagnetic storm (Davidson, 1940) was followed by other blackouts such as the famous collapse of the Hydro-Quebec system in Canada (Bolduc, 2002; D. H. Boteler, 2013) and the blackout in Malmö in Sweden during the Halloween storm 2003 (Pulkkinen et al., 2005; Rosenqvist et al., 2005; Wik et al., 2009).

The threat to extensive disruptions in the electrical power supply is greatest during extreme space weather. One of the most intense geomagnetic storms ever recorded was known as the Carrington event (Carrington, 1859) and had dramatic effects on telegraph wires (D. Boteler, 2006). In 2012, an eruption of similar magnitude was released from the Sun but it missed our planet, saving our society from possible widespread electrical disruptions, damages, and blackouts together with potential enormous societal and economic consequences (Baker, 2008; Ngwira et al., 2013). Our increasing reliance on electrical power and the non-negligible probability that such an event or an even more energetic event will occur again in the future has driven the research community across the world to develop and validate modeling techniques for GICs (Dimmock et al., 2021; Love et al., 2015; Schrijver & Beer, 2014). Such models can be used for risk assessment procedures concerning space weather hazard mitigation.

An extensive review of relevant GIC studies from around the world is given by Kelbert (2019). It points out the importance of Earth's electrical conductivity on GICs flowing in the electric power grids. Many GIC studies use a 1D plane wave method which can be justified in regions far away from large lateral conductivity gradients. However, the significance of moving toward the usage of 3D induction modeling methods and models has been pointed out by Pulkkinen et al. (2017). The importance of taking into account lateral conductivity gradients to capture the enhancement of electric fields due to the so-called coast effect has been well-documented (Gilbert, 2005; Pirjola, 2013). Recent studies have also shown the importance of the inclusion of 3D effects in GIC research in general (Divett et al., 2017; Gao et al., 2021; Ivannikova et al., 2018; Lucas et al., 2018; Püthe & Kuvshinov, 2013; Rosenqvist & Hall, 2019; Torta et al., 2017).

Sweden is situated in an exposed cratonic area with very little sedimentary cover. The presence of very strong crustal conductors create large gradients in conductivity, including large contrast between very resistive continental crust and sea water and sediments. As a result, this requires a 3D approach to accurately assess the vulnerability to GICs in different regions. Rosenqvist and Hall (2019) developed a proof-of-concept modeling capability that incorporates a detailed 3D structure of Earth's electrical conductivity in a GIC estimation procedure. The model was verified based on GIC measurements from a transmission line in northern Sweden with excellent agreement. The 3D modeling shows that induced electric fields in Sweden are dominated by the ocean-land boundary, especially in southern Sweden. Thus, this region is exposed to stronger electric fields due to the combined effect of low crustal conductivity and the influence of the coast-land interface from both the east and the west.

The susceptibility of southern Sweden to GICs has also been observed in the Swedish power grid (Svenska kraftnät, 2011). Thus, Rosenqvist and Hall (2019) identified a need to validate the GIC-SMAP model in southern Sweden for it to be useful as a tool to estimate GICs in the Swedish power transmission grid and develop worst-case scenarios to mitigate the effects by preventative measures. Also, the crustal conductivity map relies more heavily on interpolation and alternative sources of data in the lack of magnetotelluric measurements in the southern region (Engels et al., 2002; Korja et al., 2002). This further supports the need for validation in this area. For this purpose, a field trial in cooperation with Svenska kraftnät (the state owned authority responsible for the Swedish transmission system) was conducted on a transmission line in southern Sweden in May 2018. In the current study, the GIC-SMAP model is further validated in the southern region based on the GIC observations during this field trial. The location of the studied transmission line was selected based on the 3D modeling results in Rosenqvist and Hall (2019) to include the coastal-effect at the ocean-land interface to investigate the importance of using 3D induction modeling methods in such areas.

After validation, the model is used to quantify the hazard of severe GICs in this particular transmission line by applying historic recordings of strong geomagnetic disturbances to the GIC-SMAP modeling framework. To quantify a worst-case scenario the GICs were also calculated based on modeled magnetic disturbances by the Space Weather Modeling Framework (SWMF) based on estimates for an idealized extreme interplanetary coronal mass ejection. The purpose of this study is to improve the prediction capability of GICs in the Swedish region

and to demonstrate the potential of GIC-SMAP to quantify the vulnerability of the Swedish power grid to strong or extreme geomagnetic disturbances and associated GICs.

## 2. The GIC-SMAP Model

The GIC-SMAP model was developed by Rosenqvist and Hall (2019) who performed 3D modeling of the geoelectric field in Sweden. The commercial finite element software COMSOL Multiphysics was used to solve the equations describing the current distribution in the ground in the frequency domain. A full 3D conductivity model was used based on a crustal conductivity map with surrounding oceans for the Fennoscandian shield (SMAP; Engels et al., 2002; Korja et al., 2002), which is described in more detail in Rosenqvist and Hall (2019). The source current was assumed to be uniform of unit amplitude, located at a 100-km height in the ionosphere. Rosenqvist and Hall (2019) shows that the assumption of a uniform source field is valid in regions that are spatially smaller than the ionospheric variations by validating the model against observed GIC measurements during a geomagnetically quiet period from a site in northern Sweden. Thus, it was shown that it is possible to derive GICs along an arbitrarily chosen path from the modeled geoelectric field according to the following.

If we consider a transmission line along a curve  $C$  the voltage is the line integral of the electric field expressed as

$$V_{H_{0x}} = \int_C \mathbf{E}_{H_{0x}} \cdot \mathbf{n} ds \quad (1)$$

$$V_{H_{0y}} = \int_C \mathbf{E}_{H_{0y}} \cdot \mathbf{n} ds. \quad (2)$$

where  $\mathbf{E}_{H_{0x}}$  is the geoelectric field induced by a uniform incident magnetic field in the south-north direction,  $\mathbf{E}_{H_{0y}}$  is the geoelectric field induced by an uniform incident magnetic field in the west-east direction (Lettinen & Pirjola, 1985),  $\mathbf{n}$  is a unit tangential vector along the curve  $C$  and  $ds$  is an infinitesimal arc length. The curvature of Earth is neglected as we assume that the distance between the nodes of the transmission line is of the order of hundreds of kilometres, which is much less than the Earth radius.

The total induced voltage  $V$  assuming a uniform incident magnetic field is then given by

$$V = V_{H_{0x}} \left[ \frac{H_x}{H_0} \right] + V_{H_{0y}} \left[ \frac{H_y}{H_0} \right], \quad (3)$$

where  $H_0$  is the amplitude of the uniform incident magnetic field applied in the modeling of the geoelectric field. Under the assumption that the magnetic field does not vary significantly in the region of the transmission line the magnetic variations  $H_x$  and  $H_y$  from a nearby magnetometer station can be used as input into Equation 3.

Finally, the GIC,  $I(\omega)$  as a function of angular frequency ( $\omega$ ), for a stand-alone power line can be calculated according to

$$I(\omega) = V(\omega)/Z, \quad (4)$$

where  $Z$  is the total impedance of the transmission line system including the earthing and line impedances.

Rosenqvist and Hall (2019) modeled the geoelectric ground response for a uniform magnetic field variation with unit amplitude ( $|H| = 1$  A/m) for a fixed set of frequencies in the range 0.001–0.1 Hz with the polarization of the inducing magnetic field in a strictly eastern direction as well as a strictly northern direction. Figure 1 shows the resulting surface electric field for the two different polarizations in southern Sweden at the period  $T = 1,000$  s.

## 3. Validation of GIC-SMAP in Southern Sweden

### 3.1. Field Trial Observations

A field trial was conducted on 24–26 May 2018 in cooperation with Svenska kraftnät on the 400 kV power line FL66 (black line in Figure 1) between Horred (H in Figure 1) and Ringhals (R in Figure 1). The transmission line was disconnected from the rest of the grid and was operating in a stand-alone mode. GIC was measured with 5,000 samples per second using a current shunt connected between the power line and a station earthed at

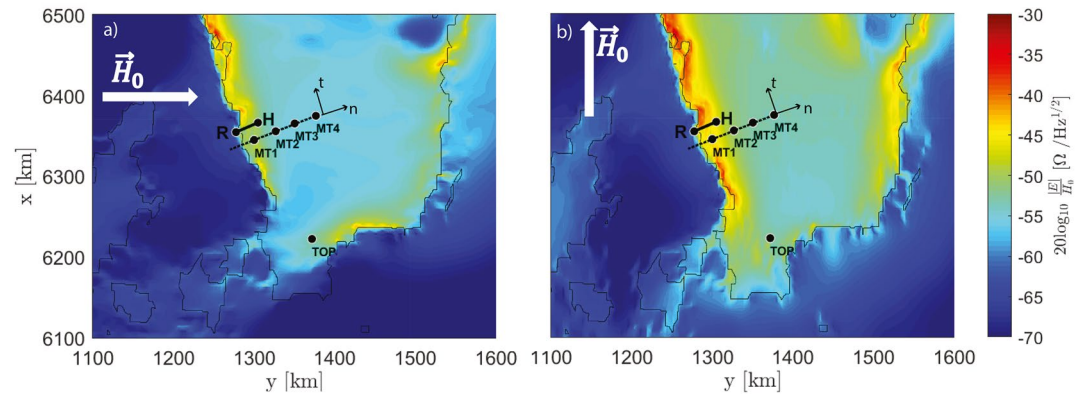


**Figure 1.** Modeled surface electric field amplitude with the polarisation of the inducing magnetic field of amplitude  $H_0$  in a strictly eastern direction (a) as well as a strictly northern direction (b) at the period  $T = 1,000$  s.

Horred. The power transmission line was short-circuited to Earth in Ringhals. Prior to the GIC experiment a full impedance scan of the power line circuit was conducted. Figure 2 shows a schematic illustration of the FL66 transmission line during the field trial as well as the circuits during (a) measurements for characterization of the power line (b) GIC measurements and (c) the resulting equivalent circuit. GICs were measured during two intervals due to other coinciding maintenance work on the power line by Svenska kraftnät. The first interval started on 24 May at 16:23 Universal Time (UT) and GICs were measured continuously for approximately 13 hr. The second interval started on 25 May at 13:06 UT and lasted approximately 16 hr.

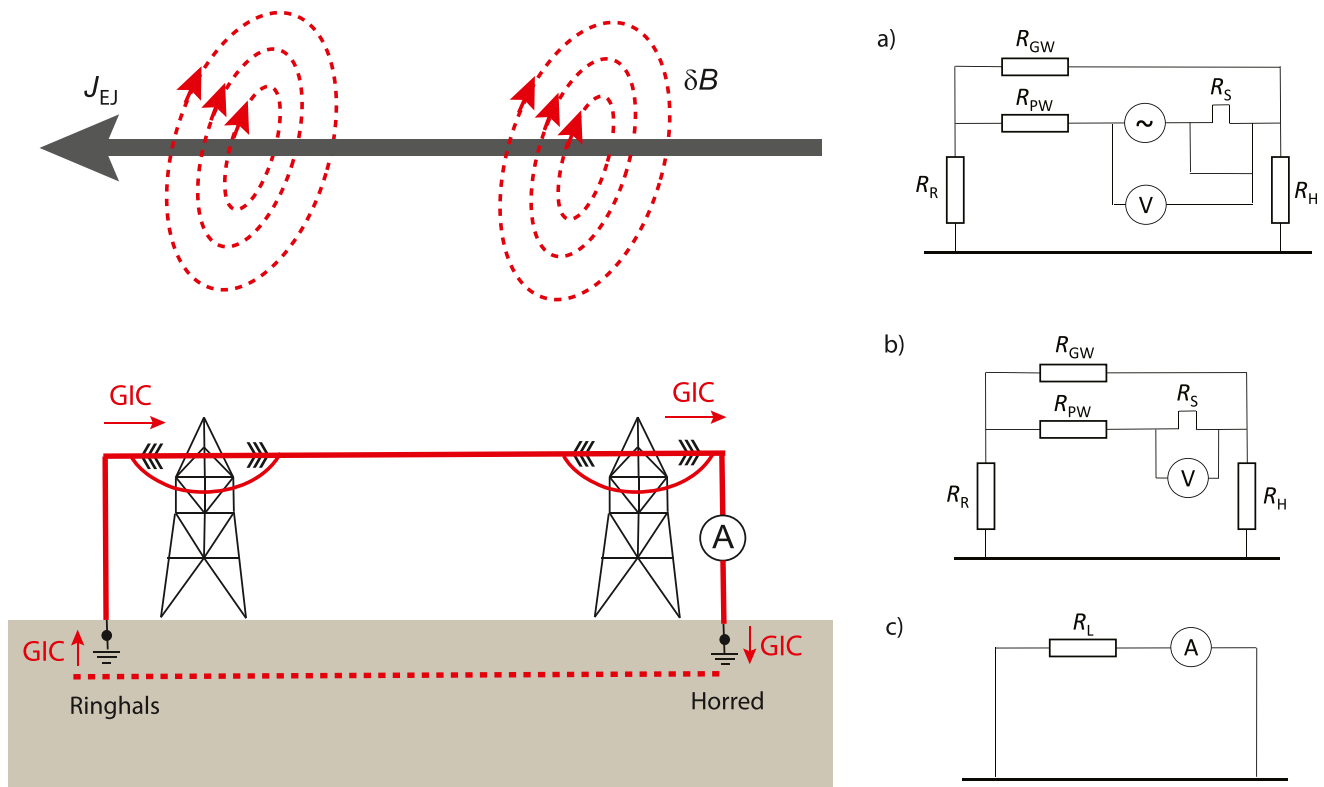


**Figure 2.** A schematic illustration of the transmission line between Horred and Ringhals during the geomagnetically induced currents field trial on 24–26 May 2018 on FL66. Circuit diagrams during (a) measurements for characterization of the power line circuit (b) GIC measurements and (c) the resulting equivalent circuit.  $R_{PW}$  denotes the calculated resistance of the phase wires connected in parallel for the test,  $R_{GW}$  the resistance of all the permanently grounded wires (for lightning protection) connecting the two stations,  $R_H$  and  $R_R$  the grounding resistances for the earth wire complexes at Horred and Ringhals respectively and finally  $R_S$  the resistance of the measuring shunt used.

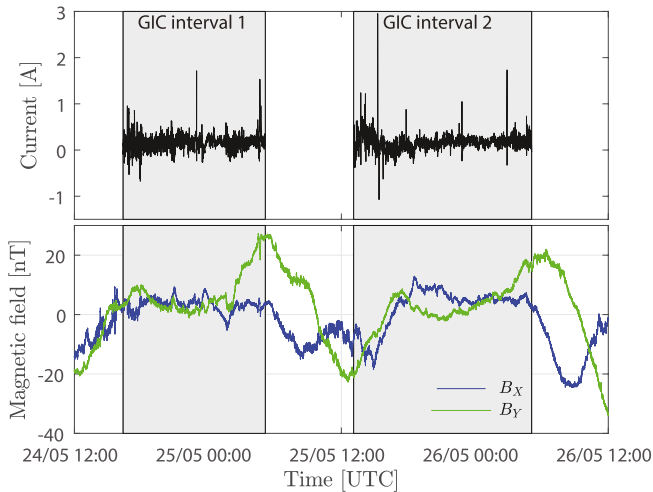


**Figure 3.** Time series of observed geomagnetically induced currents on 24–26 May 2018 during the two measurement intervals in power line FL66 (top panel) and the north-south ( $B_x$ , blue) and east-west ( $B_y$ , green) magnetic field component observed in TOP (bottom panel). The mean magnetic field values have been subtracted to exclude the Earth static field from the variations.

Moreover, four magnetotelluric (MT) stations were placed orthogonal to the coast at successively increasing distances (MT1–4 in Figure 1) separated by about 25 km and MT4 placed at approximately 100 km from the coast. The stations measure the east-west and north-south magnetic field variations with Metronix MFS-06e induction coils and the vertical component with MSF-10e induction coils. Two orthogonal electric fields oriented in the coordinate system are measured by the non-polarizing PbPbCl electrodes EFP-06 from Metronix. Magnetic observations from a three-axis fluxgate magnetometer operated by the Swedish Institute of Space Physics in Tormestorp (TOP in Figure 1) at one second resolution are also available.

Figure 3 (top panel) shows the observed GIC in power line FL66 during the two measurement intervals (black line). Data is decimated to 1 Hz using a low-pass Butterworth filter of the fourth order. The simultaneously observed north-south ( $B_x$ ) and east-west ( $B_y$ ) components of the magnetic field observed at TOP are also shown by the blue and green lines, respectively. The magnetic field shown in the bottom panel exhibits variations of around  $\pm 20$  nT, typical for daily quiet time variation. Nevertheless, the quiet time variations is pertinent to validate the local conductivity parameters and the model of the transmission line.

### 3.2. Model Validation

To model the GIC we can use Equations 1–4 in Section 2. First of all, we calculate the magnetic field amplitudes from the time series measured by the MT2 station (MT2 in Figure 1) by using a conventional Fast Fourier transform (FFT). Only one segment with the full length of the time series was used in the FFT. Prior to the FFT, spikes and data gaps introduced by the measurement equipment were removed from the magnetic field time series from the MT2 station. The data was despiked in a 30 s window using a Hampel filter and data gaps were removed by interpolation over the mean value of the data 1 s prior and after the data gap. The induced voltages in the different directions are obtained by integrating the modeled geoelectric field in Figure 1a for  $E_{H_{ox}}$  and Figure 1b for  $E_{H_{oy}}$  along the power transmission line (marked with the black line between R and H in Figure 1). As the geoelectric field is modeled for a fixed set of frequencies in the range 0.001–0.1 Hz it is necessary to interpolate both the phase and amplitude of the ground response to recreate the full GIC frequency spectrum. A sixth-order polynomial was used. The resulting modeled GIC can thus be calculated according to Equation 4. To estimate the voltage between the endpoints resulting in a measured current according to the setup in Figure 2 we need to consider both possible current shunting past the instrumentation and the serial impedance in the actual circuit. As a general consideration, we neglected all reactive properties of the circuit elements following the low frequencies of interest. In measurements the reactance in the power line/earth circuit becomes comparable to the resistive component only at frequencies on the order of 10 Hz and above. The resistance of the phase wires,  $R_{pw}$  (the three groups of wires normally carrying the power), based on available data from the grid operator was calculated to be  $0.15 \Omega$ . The resistance between the permanently grounded wires for lightning protection mounted on the pole tops,  $R_{GW}$ , connecting the stations was  $0.89 \Omega$ . The resistance of the measuring shunt during the field trial was  $R_s = 0.01 \Omega$ . Using the measured resistive component of  $0.54 \Omega$  it was deduced that a combined grounding resistance for the earth wire complexes at Horred and Ringhals ( $R_H$  and  $R_R$ ) was  $0.66 \Omega$  at the occasion. This value is slightly higher than the last official measurement ordered by the grid operator but well below “worst case” results in the past. Solving the actual measurement circuit (Figure 2b) for an effective serial resistance (Figure 2c) results in the power grid model

$$Z = R_L, \quad (5)$$

where  $R_L = 0.94 \Omega$ . The technical details and the measurement protocols concerning the national power grid are made available to us exclusively in agreement with Svenska Kraftnät and can therefore not be reproduced in detail.

Figures 4a and 4b shows the observed (black) and predicted (red) GIC time series for the two measurement intervals shown in Figure 3. Predicted GIC based on a 1D model of the conductivity in the region is also shown



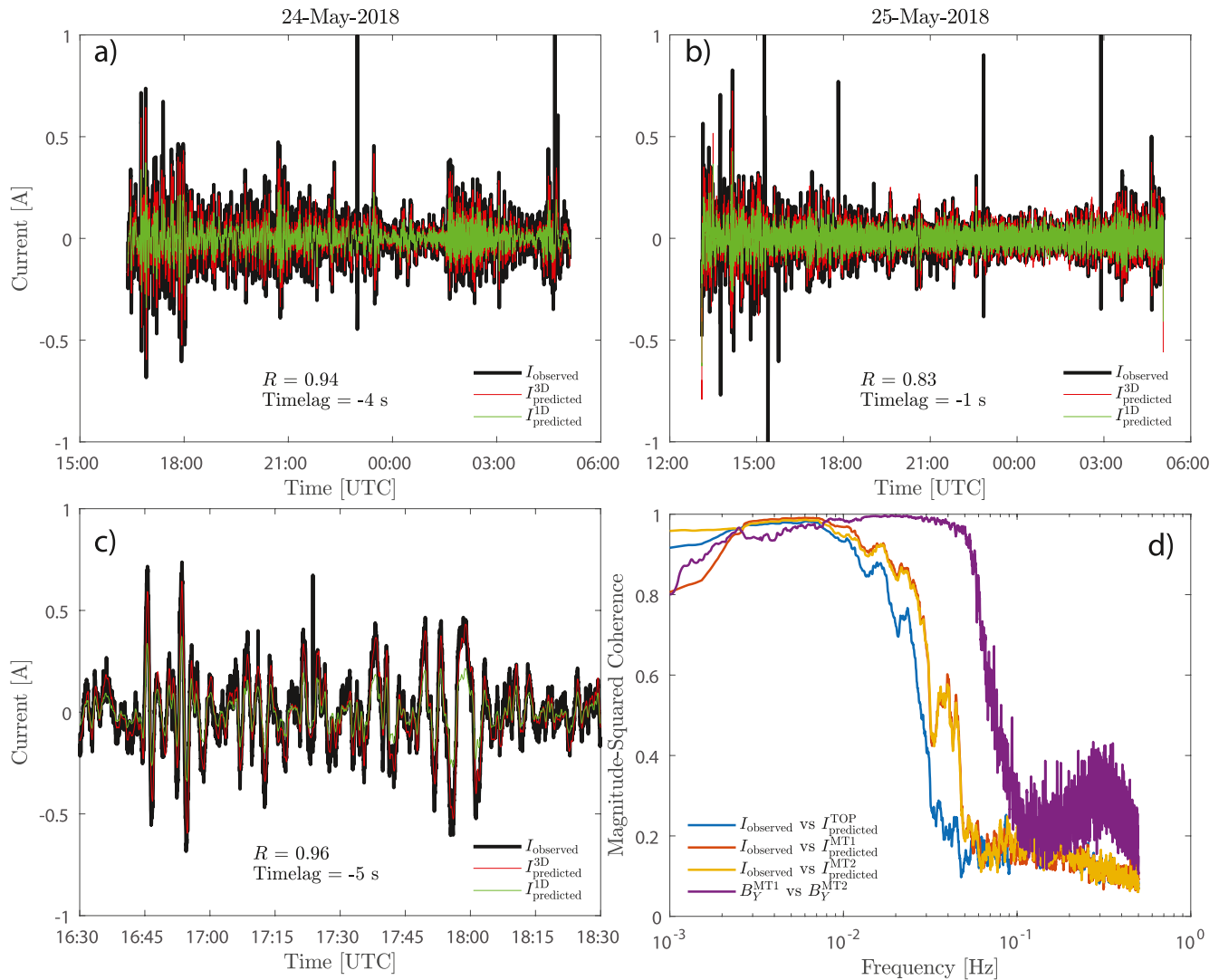


**Figure 4.** Time series of observed (black) and predicted (3D predictions in red and 1D predictions in green) geomagnetically induced currents time series in power line FL66 in southern Sweden for the first (a) and second (b) measurement interval respectively. Two hours in the first interval is shown in (c) and (d) shows the coherence between observed GIC and predicted GIC based on different magnetic field measurements (blue-TOP, red-MT1, yellow-MT2). The coherence between the  $B_Y$  component of the magnetic field measured at MT1 and MT2 is also shown in purple. The correlation coefficient,  $R$ , and the timelag where the cross-correlation is maximum of the observed and predicted (3D) timeseries are also noted in the figures.

in green. The 1D model is based on SMAP in the middle of the transmission line ( $\sigma_1 = 3.2 \cdot 10^{-4}$ ,  $\sigma_2 = 0.0021$ ,  $\sigma_3 = 0.0023$  and  $\sigma_\infty = 0.001$  following the conductivity model in Rosenqvist and Hall (2019)). An inverse Fourier transform was used on the predicted spectra to reconstruct the original GIC time series (weighted by a Hanning window). The observed GIC data were band-pass filtered between 0.001 and 1 Hz using a second-order Butterworth filter which corresponds to the relevant frequency interval for GIC disturbances in the power grid (Oyedokun et al., 2019; Pulkkinen, 2003).

Figure 4 shows that the GICs mainly fall in a range between  $\pm 0.75$  A, with some small individual spikes around 1A. We believe these short-term spikes are due to interference from a nearby parallel powerline (FL67) which was operating in normal mode during the fieldtrial and are not true GICs. This is also why they are not captured by any of the modeled GICs. From the time series, it is evident that the GICs based on the 3D model follow the measured signal closely. The favorable agreement is even more evident in panel c which shows a shorter time interval. An interesting result is that the 3D model yields higher amplitude GICs (red line) compared to the GICs modeled with the 1D model (green line). This is explained by our proximity to the coastal area with significant

lateral conductivity gradients, which results in a amplification of the geoelectric field across the transmission line as seen in Figure 1. As the 1D model cannot account for this it underestimates the predicted GICs by about 50%.

What is encouraging here is that the modeled signal appears to match its measured counterpart across the relevant temporal scales. Panel d further investigates this by investigating the coherence between observed GIC and predicted GICs based on different magnetic measurements. The blue line is the coherence between observations and predictions based on magnetic measurements from TOP, the red line based on magnetic measurements from MT1, and the yellow line based on magnetic measurements from MT2 respectively. While the coherence is close to one for lower frequencies it can be seen that the coherence starts to drop around 0.02 Hz. One explanation for this is that pulsations in this frequency band (Pi1 and Pc1) are rather rare and occur mainly during active periods such as substorms. Thus, often there is not much signal in the range between approximately 0.05 and 5 Hz which is also called the MT dead band (Chave & Jones, 2012; Egbert & Livelybrooks, 1996). This is also visualized by the drop in coherence between the magnetic field  $B_y$  component in the adjacent stations MT1 and MT2 (purple line). It can be seen that the coherence between the observed and predicted GIC drop somewhat before the MT dead band. The reason for this is not clear but could either be due to enhanced noise at higher frequencies in the measured GIC and/or modeling errors due to an inaccurate representation of the ground properties at depths important for frequencies above 0.02 Hz. Another interesting feature is the drop in coherence for lower frequencies (from 0.001 to 0.003 Hz) between observed and predicted GIC based on magnetic measurements from MT1 (red line) while a similar drop is not seen between observed and predicted GIC based on magnetic measurements from MT2 (yellow line). This is also true for the coherence between the MT1 magnetic field and the other stations which indicates a lower quality of the measurements at MT1.

In Rosenqvist and Hall (2019) a similar comparison between observations and model predictions was made for a transmission line located across the Skellefteå ore district. In that case, the observations were lagged about 60 s compared to the predictions possibly due to an inaccurate representation of the conductivity in the lower layer of SMAP in the Skellefteå ore region. For this site the timelag where the cross-correlation is maximum of the observed and predicted (3D) timeseries (noted in Figures 4a–4c) is only a few seconds which indicates that also the phase shift is rather well represented by the model in this region.

The modeled impedance tensor profiles along the MT survey line in Figure 1 (marked with dashed line) have also been compared with the impedance values evaluated at each MT location from the measurements during the field trial. In Rosenqvist and Hall (2019) it was shown that inland of  $s > 50$  km from the coast, the off-diagonal tensor components are dominant, indicating a 1D dimensionality. For 1-D environment diagonal components of the impedance tensor are zeros and main off-diagonal components are the same with opposite sign. Moving toward the coast, the impedance increases due to the enhanced effect from the coastal conductivity contrast. In this region the amplitude of the diagonal components becomes comparable to the off-diagonal indicating strong 3D effects. The MT transfer functions in terms of the impedance tensor have been estimated based on data from the four MT stations using the robust MT data processing algorithm described in Smirnov (2003). For all stations, the magnetic field from MT2 was used since this data set had the lowest level of noise. Figure 5a shows the amplitude of the impedance tensor off-diagonal component  $Z_{nt}$  for the four MT sites (MT1-black line, MT2-red line, MT3-green line and MT4-blue line).

Figure 5b shows the modeled off-diagonal component  $Z_{nt}$  for periods  $T = 1,000$  s (green line),  $T = 100$  s (red line), and  $T = 10$  s (black line). The coast is located at  $s = 0$  and the cross-section along the MT survey line is aligned perpendicular to the electromagnetic strike direction, for example, the conductivity does not change along the strike direction  $t$  but mostly in the  $n$  direction. The coastal effect is seen in the modeling by the gradual increase of the impedance with decreasing distance to the coast. The effect is stronger for longer periods (green line) and extends further inland, as the extent of the effect is proportional to the skin depth. We see an enhancement of the modeled impedance of about a factor of 3 at the coastline for  $T = 1,000$  s (green line) compared to at 100 km inland. The corresponding observed values based on the MT measurements from Figure 5a are plotted with circles and errorbars for each MT station with respect to the distance from the station to the coast. It is evident that the modeled and measured impedances are in relatively good agreement for all three periods but the enhancement expected by the coastal effect is not clearly present in the measurements. The impedances estimated at MT1, the station closest to the coast, does not show the enhancement for  $T = 100$  s and  $T = 1,000$  s expected by the coastal effect that is observed in the modeled results. On the contrary, the observed impedances are somewhat lower for MT1 than for the rest of the stations. However, the comparison between modeled and observed induced current in

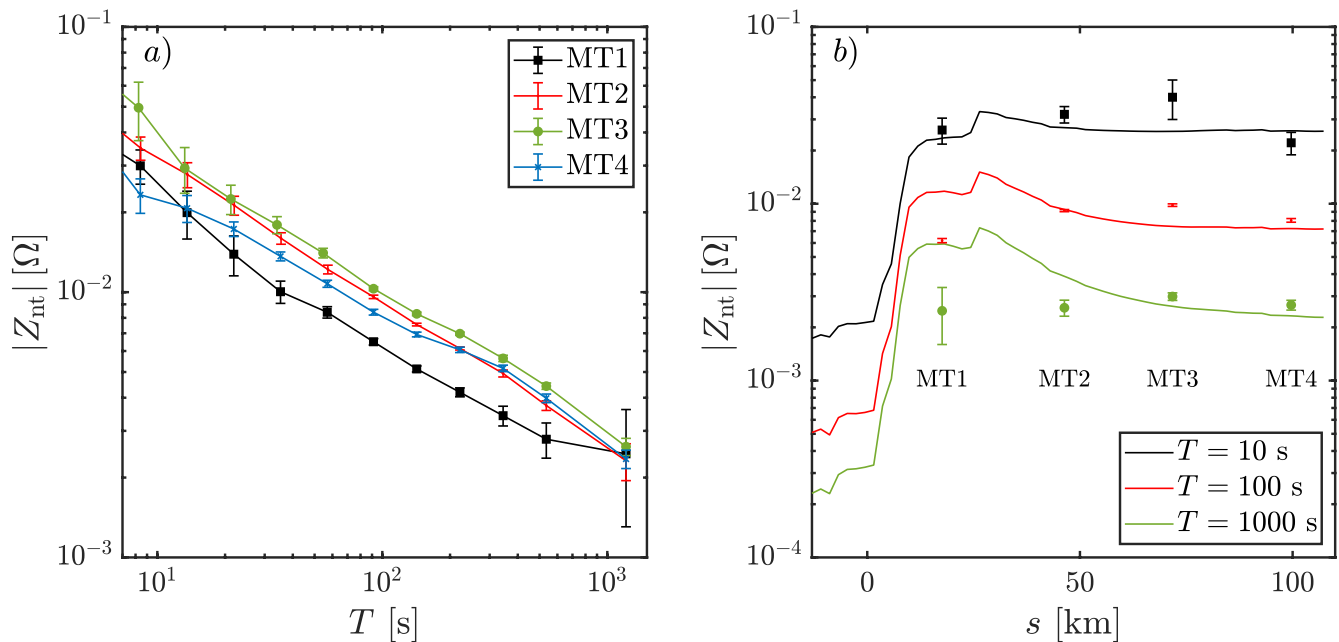


**Figure 5.** (a) Impedance for the off-diagonal component  $Z_{nt}$  based on data from the four different Magnetotelluric (MT) stations (b). Profiles of the modeled impedance along the line intersecting the MT stations shown in Figure 4 for periods  $T = 1,000$  s (green),  $T = 100$  s (red), and  $T = 10$  s (blue) respectively. The coast is located at  $s = 0$ . The corresponding values based on measurements from the MT stations are shown with dots and errorbars.

the transmission line FL66 clearly show that a 3D model taking into account the enhancement due to the coastal effect is needed in order to reproduce the observed induced current (see Figure 4). Unfortunately the data in MT1 is suffering from significantly more noise than the rest of the stations, which was indicated by a lower coherence between the magnetic and electric field at this site compared to the other sites. This resulted in the removal of a larger number of data ensembles in the coherence sorting criteria according to Smirnov (2003). That the MT1 measurement contained more noise is also indicated by the larger error bars of the impedance tensor at longer periods (above 300 s) shown in Figure 5a. Figure 5 shows that the uncertainties are smallest around a period time of around 100 s and increases for both shorter periods (the MT dead band) and longer periods (too few periods to establish reliable statistics). Moreover, static effects due to local ground properties at each site could pose a problem in the above analysis and obscure potential coastal effects in the data analysis.

#### 4. Historical Geomagnetic Disturbances

In Section 3.2 we have verified that the model is in good agreement with observational data for both measurement periods. However, geomagnetic activity during the field trial was quiet for the observational intervals. The observed maximum GICs are of the order of 1 A and is far from hazardous to power grid operations. If one assumes that GIC scales linearly with the magnitude of the magnetic variations (see e.g., Tóth et al. (2014)) the validated model can be used to predict the GIC in the FL66 power line during periods of high activity. Such an assumption can be considered relevant if the source fields are homogeneous along the power line.

In this section, magnetic recordings of historical geomagnetic storms together with the GIC-SMAP model will be used to predict the peak GIC in terms of the maximum of the absolute value of the current in the FL66 power line. The extended SWPC-CCMC (Space Weather Prediction Center Community and Coordinated Modeling Center) validation suite (Welling et al., 2018) has been used for this purpose. The storm of 7–8 September 2017 has been added to the list as its geomagnetic response over Fennoscandia has been studied previously (Dimmock et al., 2019). The 14 geomagnetic storms are listed in Table 1 together with maximum values of different solar and geomagnetic activity indices (F10.7, Kp, AE, and SYM-H). Magnetic recordings based on 60 s resolution data from geomagnetic latitudes similar to the geomagnetic latitude of the FL66 transmission line (around  $55.4^\circ$  corresponding to  $57^\circ$  geographic latitude) have been selected from the INTERMAGNET global network of observatories. To study the latitudinal dependence in Sweden, magnetic data from the observatories in Sweden have also



**Table 1**  
*List of Studied Historical Geomagnetic Storms (Dimmock et al., 2019; Welling et al., 2018)*

Number	Event start	Extent(hr)	F10.7 (sfu)	Kp	AE (nT)	SYM-H (nT)
1	29 Oct 2003 06:00 UT	24	275.4	9°	4056.0	−391.0
2	14 Dec 2006 12:00 UT	36	90.5	8+	2284.0	−211.0
3	31 Aug 2001 00:00 UT	24	203.0	4°	959.0	−46.0
4	31 Aug 2005 10:00 UT	26	86.0	7°	2063.0	−119.0
5	05 Apr 2010 00:00 UT	24	79.0	8−	2565.0	−67.0
6	05 Aug 2011 09:00 UT	24	113.0	8−	2611.0	−126.0
7	17 Mar 2015 02:00 UT	34	116.0	8−	2298.0	−234.0
8	22 Jul 2004 06:00 UT	162	178.4	9−	3632.0	−208.0
9	07 Nov 2004 00:00 UT	60	138.1	9−	3360.0	−394.0
10	30 Mar 2001 12:00 UT	48	257.2	9−	2407.0	−437.0
11	17 Mar 2013 00:00 UT	48	124.5	7−	2689.0	−132.0
12	06 Apr 2000 12:00 UT	48	178.1	9−	2481.0	−320.0
13	15 May 2005 00:00 UT	24	105.2	8+	2051.0	−305.0
14	8 Sep 2017 00:00 UT	48	130.4	8+	2677.0	−142.0

been used to evaluate the peak GIC in the FL66 power line during the historic storms. The selected stations used in the analysis together with their geographic and geomagnetic latitude are shown in Table 2. Figure 6 shows the geographic location of Horred together with the locations of the selected observatories. The geographic latitude of Horred is shown by the dashed line.

Figure 7a shows the maximum horizontal magnetic field time derivative ( $dB_H/dt$ ) during the 14 geomagnetic storms listed in Table 1. The GMD event number on the  $x$ -axis corresponds to the order in Table 1, and the line color indicates the different magnetometer stations. The GICs, shown in Figure 7b, are modeled in the FL66 power line under the assumption that the station recordings took place uniformly around the power line location. Similar to panel a, we plot the peak GIC for each storm and at each magnetic station. For some of the storm intervals, magnetic data was missing in some of the stations which explains why some peak values are missing (for example LYC data is missing for GMD event number 8 and 9). The color scale relates the amplitudes of  $dB_H/dt$  and GICs to possible impacts, as described below.

To assess the impact of the storms the magnitudes in Figure 7 should be put in relation to associated power grid effects. Marshall et al. (2011) has determined risk level thresholds based on the “GIC index” from a wide data set of worldwide documented occurrences of power network faults due to GICs. The thresholds for the  $GIC_x$  index (based on the northward magnetic field component) associated with a fault occurrence probability is found in Table 3. The scale for the  $GIC_y$  (based on the eastward magnetic field component) is higher than for  $GIC_x$ . An explanation can be given in terms of the standard deviation of the eastern component that is generally lower than that of the northern component (Tozzi et al., 2019). It could also be due to 3D conductivity distribution effect which is not random, but large scale lithospheric anomalies exist.

Based on communications with the US electric power transmission industry, the solar shield project (Pulkkinen et al., 2010) found that it is useful to categorize the peak GIC in three broader categories of small/medium/large. While the boundaries between these categories are operator dependent, a rough classification of the GIC boundaries can be found in Table 4. The thresholds of this broader classifications are more or less in accordance with the low/moderate/high thresholds for the  $GIC_x$  index in Table 3.

Observed power grid effects in Sweden from 1982 to 2012 have been associated with magnetic field measurements between 55° and 65° north. A rough classification of the relation between the horizontal magnetic field ( $dB_H/dt$ )

**Table 2**  
*List of Selected Magnetic Observatories Used in the Analysis of Geomagnetically Induced Currents (GIC) in FL66 During Historical Storms*

Station	Geographic latitude	Geomagnetic latitude
Eskdalemuir (ESK)	55.32°	53.19°
Novosibirsk (NVS)	55.03°	50.81°
Magadan (MGD)	59.97°	53.91°
Fort McMurray (FMC)	56.66°	64.53°
Uppsala (UPS)	59.9°	56.34°
Lycksele (LYC)	64.61°	61.46°
Abisko (ABK)	68.35°	65.18°

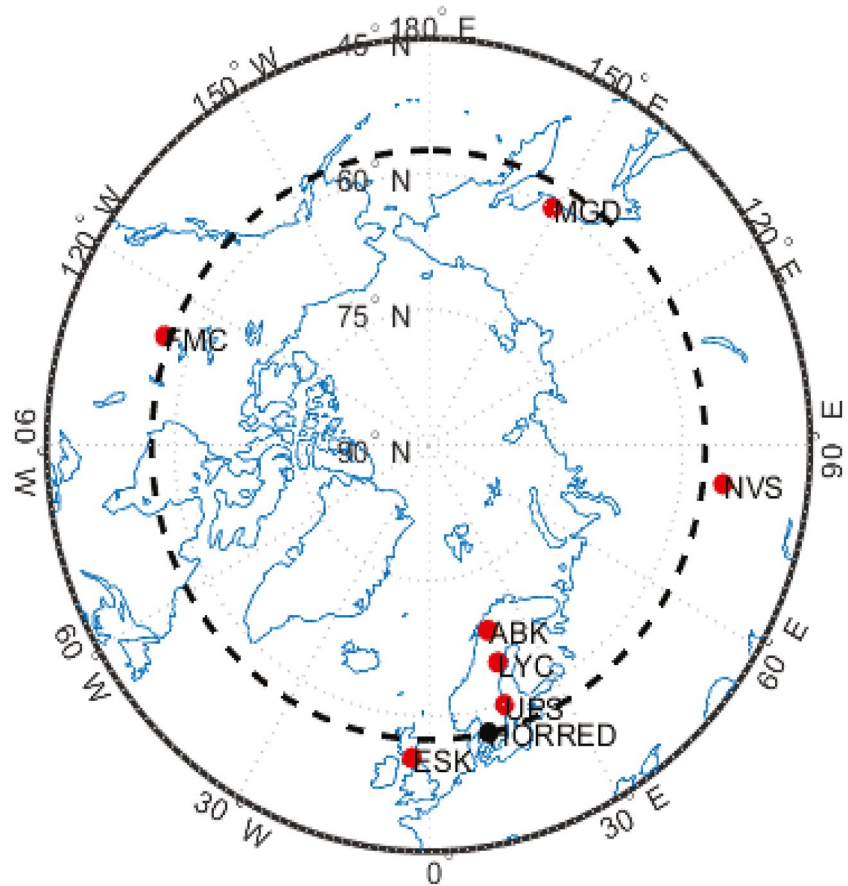


**Figure 6.** Location of the observatories used in the analysis of major GMDs in red. The location of the Horred field trial is marked in black and the geographic latitude of Horred is marked with the dashed line.

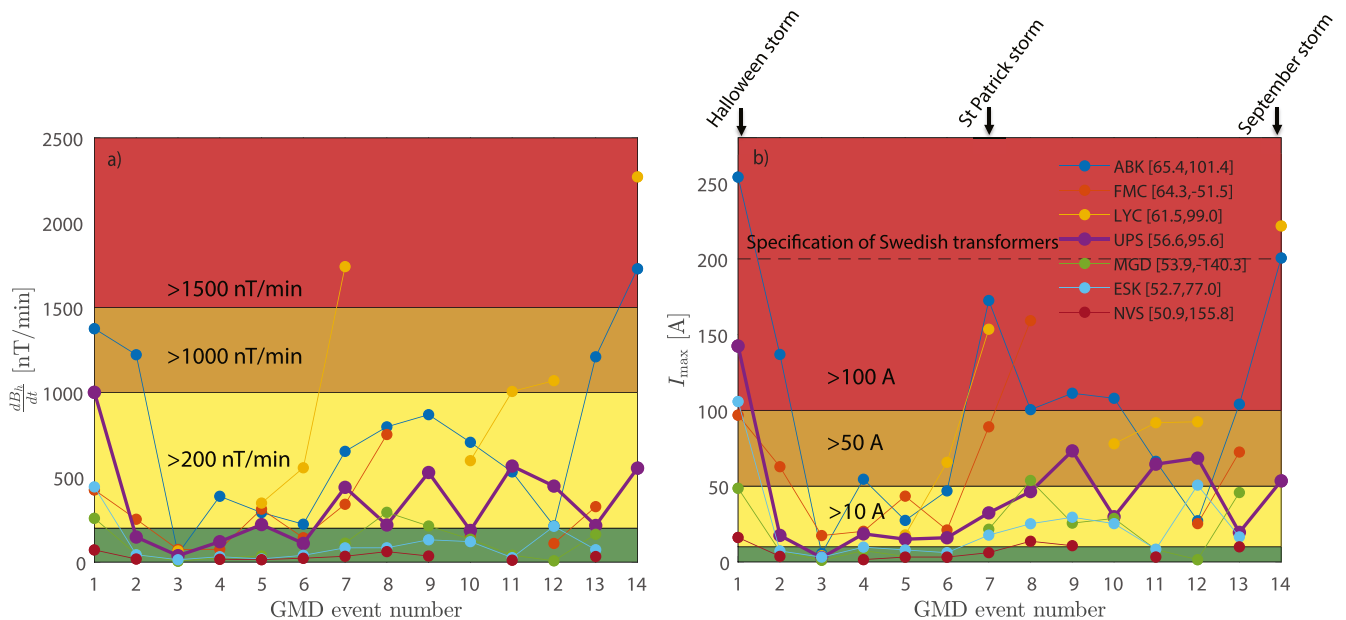


**Figure 7.** Maximum horizontal magnetic field variation for different magnetometer stations during the historical geomagnetic disturbances (GMDs) (a) and maximum GIC in the FL66 transmission line (b). The color scale shows the rough classification of the  $\frac{dB}{dt}$  and GIC associated power grid effects.

**Table 3**  
Risk Level Thresholds for the Geomagnetically Induced Current (GIC)<sub>x</sub>  
Index Following Marshall et al. (2011)

Size	Fault occurrence probability	GIC <sub>x</sub>
Very low	<5%	≤25 A
Low	5%–35%	25–50 A
Moderate	35%–65%	50–125 A
High	65%–95%	125–300 A
Extreme	>95%	>300 A

and effects in the power grid is found in Table 5. The use of  $dB_H/dt$  as an approximation for GIC works well in Sweden as it lies on a very resistive terrain block. However, other proxies may be more useful in other regions or countries as the relationship between  $dB_H/dt$  and  $E$  (which is the primary factor determining the scale of the GICs) depends on the local geological properties (the frequency dependent magnetotelluric transfer function), see for example, (Juusola et al., 2020).

The thresholds of ( $dB_H/dt$ ) according to Table 5 and GIC according to Table 4 are color-coded in Figure 7. Most of Swedish transformers are three-legged with a good resistance to GICs. At full load they are designed to withstand a 200 A direct current for at least 10 min (private communication with Johan Setréus at Svenska Kraftnät). This GIC specification of Swedish transform-

ers is shown by the dashed line in Figure 7 (left panel). The maximum ( $dB_H/dt$ ) and GIC for the 14 historical GMDs show an expected clear increase with latitude with the highest magnitudes for both  $dB_H/dt$  and GIC being observed in the Abisko (ABK) station for the majority of the events. The maximum GIC based on magnetic observations closest to the FL66 location, corresponding to UPS (purple line), only reach above the highest threshold for the Halloween storm (number one in Table 1). During this storm, a famous large-scale blackout occurred in the Malmö region at 2007 UT on the 30th of October (Pulkkinen et al., 2005; Rosenqvist et al., 2005) and the estimated maximum GIC in the FL66 power line occur at the same time.

For the rest of the events, the maximum GICs are within the small and medium-range for this latitude. However, disturbances were observed in the Swedish power grid for the storm on the 17th of March 2015, the so-called St. Patrick storm (number 7 in Table 1) as well as on 8th of September 2017, during the so-called September storm (number 14 in table 1). In mid-Sweden on T8 Midskog close to Östersund at 17:33 UT on 17th of March 2015, a transformer tripped on the slow-step for an unknown reason. It was associated with the geomagnetic disturbances during this time. Similarly, at 00:29 UT on the 8th of September 2017 a transformer tripped on the slow-step on T1 Bandsjö close to Sundsvall. Figure 7b shows that the maximum GIC for these storm reached levels above the 100 A threshold and close to or above the 200 A specification for Swedish transformers based on the ABK and LYC observations at higher latitudes. The maximum GIC and  $dB_H/dt$  at LYC, which is located only 200 km from the locations of the transformer impacts, occur simultaneously as the reported impact and the peak  $dB_H/dt$  reached above the highest threshold in Table 5. However, the exact location of the impact is most probably dependent on specific network characteristics in this area.

## 5. A “Perfect” Storm

Tsurutani and Lakhina (2014) used observational records and qualitative physical arguments to estimate solar-wind parameters of an idealized extreme interplanetary coronal mass ejection (ICME). The arrival of such an ICME on Earth is argued to create a “perfect” geomagnetic storm with an intensity greater than the famous Carrington event. The ICME velocity is estimated to  $\sim 2700 \text{ km s}^{-1}$  at Earth, which under conditions for a maximum ICME shock means that the ICME can transit from Sun to Earth in only  $\sim 12 \text{ hr}$ . Using an empirical scaling law between the ICME speed and magnetic field in the magnetic cloud and assuming the magnetic field to be orthogonal to the solar wind flow, the interplanetary magnetic field (IMF) magnitude change is estimated to  $B_z$  of 127 nT. The solar wind density is estimated to  $20 \text{ cm}^{-3}$  and the magnetopause would be compressed to  $\sim 5.0 R_E$  from the center of the Earth. The estimated maximum sudden impulse intensity  $\Delta H$  is predicted to  $\sim 234 \text{ nT}$  and  $dB/dt$  to  $1,800 \text{ nT/min}$  ( $30 \text{ nT/s}$ ). These estimated extreme solar wind conditions have been used

to drive a coupled magnetohydrodynamic-ring current-ionosphere model of geospace to simulate the response of the system to the sudden impulse (SI) associated with the ICME arrival (Welling et al., 2020). Since the present study addresses the sudden impulse we do not consider substorm effects, which can also create large geomagnetic disturbances at these latitudes but around the midnight sector (Viljanen et al., 2006). Two separate orientations of the IMF were considered, corresponding to a southward and a northward turning of the IMF to 127 nT. The modeling was performed with the SWMF and the details of the modeling method can be found in Welling et al. (2020).

**Table 4**  
Rough Classification of Geomagnetically Induced Current (GIC) Magnitude

Size	GIC amplitude
Small	10–50 A
Medium	50–100 A
Large	>100 A

**Table 5**  
*Risk Level of Power Grid Effect in Sweden in Relation to  $dB_H/dt$ <sup>a</sup>*

Range	Impact
$dB_H/dt$ down to 30 nT/min	Detectable GIC reminiscent of grounding faults
$dB_H/dt > 200\text{--}500$ nT/min	Temporary loss of individual transformers
$dB_H/dt > 1,000$ nT/min	Temporary loss of 400 kV lines for central Sweden
$dB_H/dt > 1,500$ nT/min	Large voltage fluctuations, temporary loss of 400 kV and 220+ kV lines across Sweden.

<sup>a</sup>Wintoft P.S. Arnborg, H. H Lundstedt, M. Wik, Solar conditions during large ground geomagnetic  $dB/dt$  events, European Space Weather Week 10 Nov 2013.

The simulated response of the “perfect” sudden impulse with SWMF predicts magnetic field variations above the 1,800 nT/min found by Tsurutani and Lakhina (2014) and surpass those of historically recorded extreme events.

Using the same argument as in the previous section, that GIC scales linearly with the magnitude of the magnetic variations, the modeled magnetic field variations from the SWMF run during the sudden impulse phase can be used to predict a “worst-case” GIC magnitude in the FL66 power line with the GIC-SMAP model. The magnetic field variation during the sudden impulse phase in a latitudinal band around the location of FL66 (55, 57, and 60° latitude) have been investigated. The sudden impulse phase is covering a period of 2 minutes before the ICME shock arrival through 5 minutes afterward. To study the dayside and nightside shock-related disturbance, the maximum values in all longitude sectors with a spacing of 5° have been evaluated. Figure 8 shows virtual magnetometer magnetic field (a) and magnetic field variation (b) in the north-south direction for stations at 57° latitude (corresponding to FL66 location), 2 minutes before shock arrival through 5 minutes afterward for the southward IMF case. Stations are arranged from local noon (longitude 50°) and in five increasing longitudinal steps to 300° longitude. The corresponding modeled GIC time series predicted with the GIC-SMAP model in the FL66 transmission line is shown in Figure 8c. The east-west components of the magnetic field (not shown) also contributes to the GICs but they are considerably lower. The maximum  $dB/dt$  at 57° is ~9180 nT/min and occurs as expected at local noon. The maximum GIC occurs at local noon on the dusk side and is around 200 A.

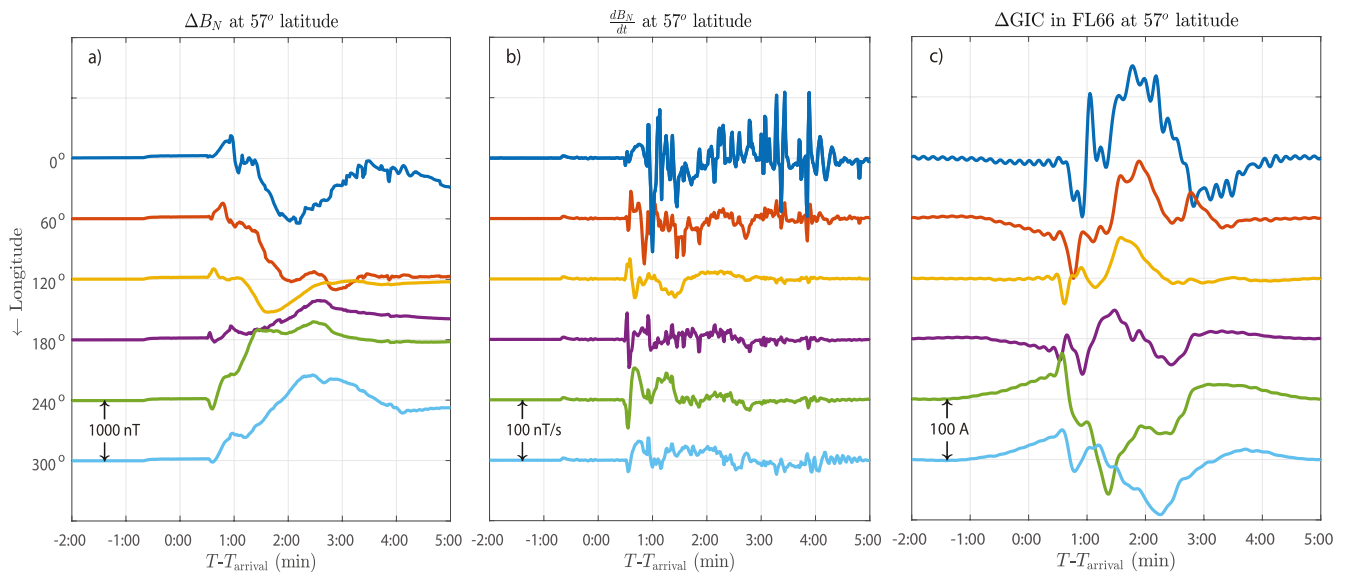


**Figure 8.** Virtual magnetometer magnetic field (a) and magnetic field variation (b) in the north-south direction for stations at 57° latitude, two minutes before shock arrival through five minutes afterward for the southward interplanetary magnetic field case. Stations are arranged from local noon (longitude 50°) and in five increasing longitudinal steps to 300° longitude. (c) The corresponding modeled geomagnetically induced current (GIC) time series in the FL66 transmission line. The black arrow in the lower-left of each frame shows the scale of the perturbations.

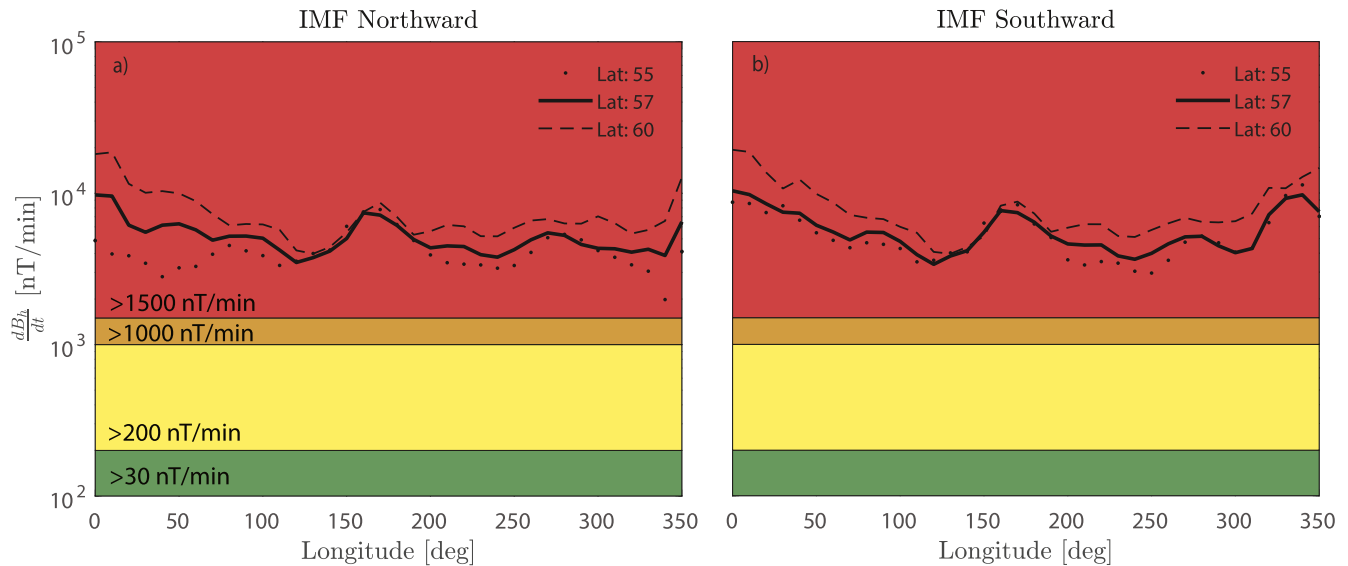


**Figure 9.** Maximum horizontal magnetic field variation for different longitude sectors during the modeled SI event for a northward directed interplanetary magnetic field (IMF) (to the left) and a southward directed IMF (to the right). The y-axis is on a logarithmic scale. The color scale shows the rough classification of the  $dB/dt$  associated power grid effects.

However, as the GIC is associated with the sudden impulse phase it lasts only for a few minutes which is still within what Swedish transformers are rated for.

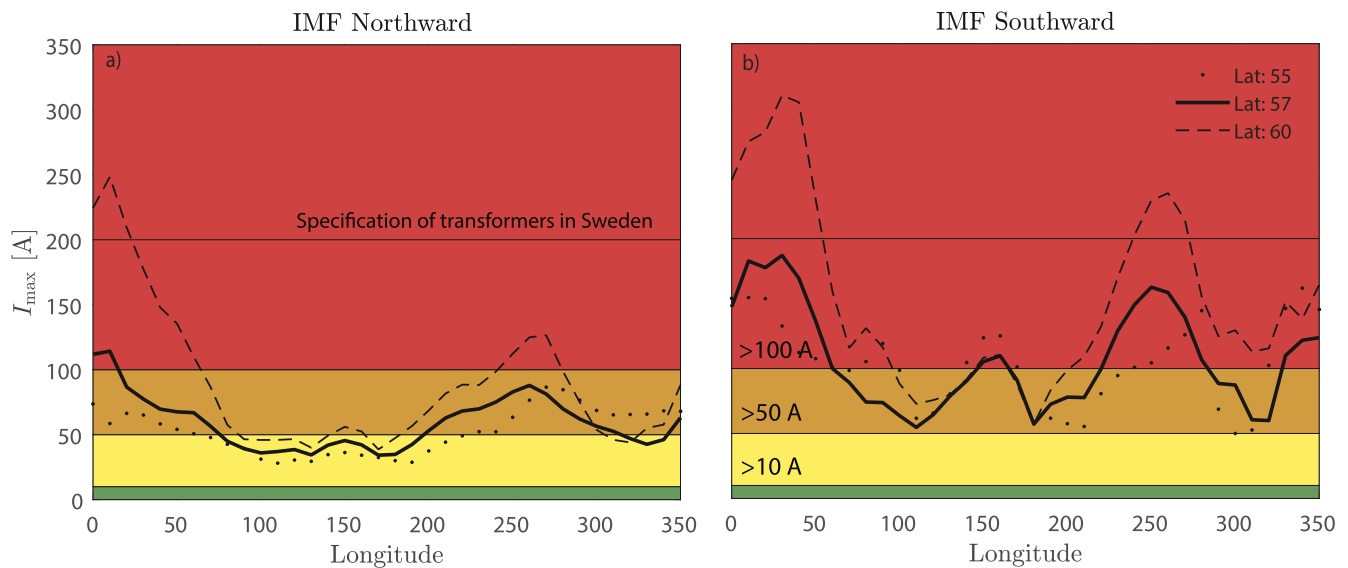
Figure 9 shows the maximum horizontal magnetic field variation for different longitude sectors during the modeled SI event at 55° latitude (dotted line), 57° latitude (solid line), and 60° latitude (dashed line) for a northward turning IMF (a) and a southward turning IMF (b) respectively. The color scale show the rough classification of the  $dB_h/dt$  associated power grid effects according to Table 4. Note that the y-axis is plotted on a logarithmic scale in order to visualize the different  $dB_h/dt$  thresholds. The  $dB_h/dt$  is largest at the dayside which is expected as the modeling only includes the sudden impulse phase of the storm. For the case of a northward turning IMF the maximum  $dB_h/dt$  at 57° latitude is 8700 nT/min and 9180 nT/min for the southward turning case. These values are well above the estimated value of 1,800 nT/min according to Tsurutani and Lakhina (2014). They exceed the highest threshold of risk levels according to Table 4 by an order of magnitude. It is also worth pointing out that regardless of the longitude, the upper threshold is always exceeded. This indicates that at these latitudes there is a significant hazard to ground-based systems regardless of magnetic local time sector. Also, it is likely that this risk also extends over a large range of latitudes.

Figure 10 shows the calculated maximum GIC in FL66 for different latitudes for the modeled SI event for a northward IMF (a) and a southward IMF (b) respectively. The maximum GIC is strongly dependent on magnetic local time (MLT) with the largest values in the dusk-noon sector for the case of northward IMF and on the dusk to dawn sector for the southward IMF. The maximum GIC in FL66 in the studied latitudinal band exceeds 250 A for IMF  $B_z > 0$  and 300 A for  $B_z < 0$  which is well above the 200 A specification for Swedish transformers. For the northward case, there is a sharp gradient in maximum GIC at noon. The reason for this gradient is due to a sharp decrease in the modeled magnetic field at the dawn side of noon compared to the dusk side of noon in the SWMF run. The reason for this discontinuity at noon is currently not established. It is beyond the current scope and will be addressed in a subsequent investigation.

## 6. Discussion and Conclusion

The present study has utilized and expanded on the modeling capability by Rosenqvist and Hall (2019) which incorporates a 3D crustal conductivity map with surrounding oceans, sea basins, and continental areas to derive the geoelectric ground response due to a uniform magnetic field. The motivation for this investigation is based on the fact that our previous work identified southern Sweden as prone to electric fields that are dominated by the ocean-land boundary. This is also relevant for other nations with comparable geological situations. As a result, it





**Figure 10.** Maximum GIC in the FL66 transmission line for different longitude sectors during the modeled SI event for a northward directed interplanetary magnetic field (IMF) (a) and a southward directed IMF (b).

is exposed to stronger electric fields due to the combined effect of low crustal conductivities and the influence of the coast-land interface from both the east and west. This makes southern Sweden possibly vulnerable to GICs, especially in coastal areas such as in areas around Oskarshamn and Malmö (Svenska kraftnät, 2011). It is highly important that the GIC-SMAP model is validated in this region to be effective as a tool to estimate GICs in the Swedish power transmission grid and develop worst-case scenarios to mitigate the effects by preventative measures. For this purpose, a field trial in cooperation with Svenska Kraftnät has been conducted in southern Sweden and the measurements have been compared with the GIC-SMAP modeling results. We have then used the model to determine the GICs from several large geomagnetic storms and also a worst-case scenario.

For the field trial of the FL66 power line, the location of the transmission line was selected based on the 3D modeling results in Rosenqvist and Hall (2019) to include the coastal-effect at the ocean-land interface. It is well established that large geoelectric fields are expected in close proximity to large conductivity gradients, and differences between 1D and 3D conductivity models may be large (Honkonen et al., 2018). This becomes a problem at some coastlines when a highly conductive seawater meets a resistive land boundary (e.g., Gilbert (2005)). In Figure 4 we directly compared 1D and 3D model outputs and observed that the peak magnitude of the GICs from the 1D model underestimates the GIC by about 50% while the 3D model was in good agreement with the measurements. One reason for this discrepancy is that 1D models can only account for conductivities as a function of depth, and therefore cannot capture coastal effects which require lateral conductivity profiles. This result indicates that in this region, 1D models are insufficient, and to accurately model GICs a fully 3D model is required. This may also be true in-land where large conductivity anomalies exist caused by graphites, sulphides and partly water in the crust and upper subsurface. Having said this, it was shown by Dimmock et al. (2019) that in some locations, 1D and 3D model differences can be small if the local geology is quite uniform. Therefore, the requirement for 1D and 3D models needs to be evaluated based on detailed knowledge of the local geological environment which will require the continuation of magnetotelluric surveying at the appropriate spatial resolution. It should be noted that the results in this study rely on the ground conductivity given by SMAP in this region. While the SMAP model is rather well-defined in the northern region of Scandinavia due to large amount of recently acquired MT data, SMAP relies more heavily on other sources of data in the south where MT measurements are more sparse. The MT measurements conducted in this study indicate that the ground in the region is somewhat more resistive (10%–20%) than what is given by SMAP. A denser net of MT surveys in southern Scandinavia is needed to validate SMAP in this region.

While a comparison between modeled impedances with impedances estimated based on MT data selected during the field trial show a relatively good agreement overall, the observations does not show indications of a coastal effect closer to the coast. However, the MT station closest to the coast (MT1), where the coastal effect was

expected to be largest, suffered from noise and thus the impedance estimation process was less reliable for this site. Also, static effects due to local ground properties at each site could pose a problem in the analysis and obscure potential coastal effects. Thus, the lack of a coastal effect in the MT analysis is inconclusive and a deeper analysis involving for example, inversion techniques to remove static effects and/or other MT techniques (Ledo et al., 2014) to achieve a better estimate at site MT1 is needed. Also additional field trials with a denser set of sites closer to the coast may be needed to experimentally show the coastal enhancement.

Under the assumption that GIC scales linearly with geomagnetic activity the validated GIC-SMAP model for the FL66 transmission line was used to predict the peak GIC based on magnetic recordings during 14 historical storms. At the relevant latitudes, around 57° degrees, of the FL66 power line, the maximum GIC exceeded 100 A only for the Halloween storm on the 30th of October 2003. The maximum GIC occurred simultaneously as the large-scale blackout in Malmö about 20:07 UT. Disturbances were also reported in the Swedish power grid on the 17th of March 2015, during the St. Patrick storm (number 7 in Table 1) and on the 8th September 2017 (number 14 in Table 1). These two impacts are associated with high levels of predicted peak GICs in the FL66 transmission line (above 100 A) based on geomagnetic data at higher latitudes where the LYC and ABK occupy. The maximum GIC and  $dB_H/dt$  at LYC, which is located only 200 km from the locations of the transformer impacts, occur simultaneously with the reported impact, and the peak  $dB_H/dt$  reached above the highest threshold in Table 4.

The field trial at FL66 was conducted during a geomagnetically quiet period, and the assumption of a uniform source field over the area of the transmission line can be considered valid. Although the magnetic field has a significant spatial variation in reality, especially during geomagnetically active periods and at high latitudes (Dimmock et al., 2020; Ngwira et al., 2015, 2018), the typical scale of localized magnetic variations during geomagnetic active periods is longer than the FL66 line which is only 30 km. We expect that the differences between the peak GIC from each of these storms is not due to the above assumption but the various levels of driving from the individual events. Nevertheless, the impacts on the ground geoelectric field based on SMAP combined with realistic source currents (Amm & Viljanen, 1999) are currently under investigation in which ionospheric equivalent currents for the September 2017 storm has been included in the COMSOL modeling.

To quantify a worst-case scenario, GICs in FL66 are predicted based on modeled magnetic disturbances by the SWMF based on estimated “perfect” ICME conditions (Welling et al., 2020). The maximum GIC is strongly dependent on MLT with peak values occurring in the dusk-noon sector. The maximum GIC predicted in FL66 based on the magnetic field at 60 degrees latitude exceeds 250 A for IMF  $B_z > 0$  and 300 A for  $B_z < 0$ . It is striking that these values are well above the 200 A specification for Swedish transformers. Thus, in the event of a “perfect” ICME such as that studied here, evidence suggests that southern Sweden may experience power grid disturbances. It should also be noted that the particular transmission line studied in this paper is relatively short and thus GICs in the Swedish power grid may be larger than the values found here.

It is important to note that the values for the extreme interplanetary conditions have been extrapolated from typical values, and the validity of linearity for certain relationships may not hold. However, in the lack of other extreme event information, these maximal conditions can be used to quantify the magnitude of terrestrial effects in the power grid. What should be noted is that the hypothetical event was modeled with SWMF for the period of the impact of the ICME upon Earth and the sudden impulse phase covering 7 minutes. While sudden storm commencements or sudden impulses can be an important source for large GICs that occur at mid-latitudes (Kappenman, 2003; Marshall et al., 2012; Zhang et al., 2015), large GICs at high-latitudes are usually associated with the rapid magnetic field variations associated with substorms (D. Boteler, 2001; Pulkkinen et al., 2008, 2005; Wik et al., 2009; Viljanen et al., 2006; Rosenqvist et al., 2005). However, this aspect is difficult to investigate since substorms remain a significant challenge for global MHD simulations (Haiducek et al., 2020) in terms of event triggering and capturing the associated small-scale dynamical ionospheric current patterns. As a result, during substorm periods, the ground magnetic field derived from global MHD tends to miss or significant under-estimate the large magnetic depressions associated with these events (Dimmock et al., 2021).

It is important to reiterate that this study applies to one individual transmission line and is not a complete representation of the vulnerability of the Swedish power grid to geomagnetic disturbances. However, it shows that the GIC-SMAP model can be a powerful predictive tool to estimate GICs in the Swedish power transmission grid and that it can be used to quantify the hazard of severe GICs for different network topologies for major

geomagnetic disturbances. The model can be used to identify critical sites that may be more prone to enhanced GICs and to determine both mitigation strategies and relevant locations for installing monitoring equipment.

## Data Availability Statement

The INTERMAGNET data and its derived data products can be obtained free of charge at [www.intermagnet.org](http://www.intermagnet.org). Data from the Tormestorp magnetic observatory (TOP) are available via the Swedish Institute of Space Physics. The Space Weather Modeling Framework is maintained by the University of Michigan Center for Space Environment Modeling and can be obtained at <http://csem.engin.umich.edu/tools/swmf>. All model results data used for this study are available via Welling et al., 2020 (<https://doi.org/10.5281/zenodo.3620786>). Requests for access to the GIC measurements used in this study can be made to the corresponding author after which the Swedish Defence Research Agency could grant a non-exclusive, non-transferable right to use the data for research purposes.

## Acknowledgments

We thank Svenska kraftnät for the collaboration with the GIC measurements from the power line FL66. We are unable to directly provide the GIC measurements and magnetotelluric data collected during the field trial. Requests for access to the measurements can be made to the corresponding author after which the Swedish Defence Research Agency could grant a non-exclusive, non-transferable right to use the data for research purposes. This work was partly supported by the Swedish Civil Contingencies Agency, grant 2016–2102. The results presented in this paper rely on the data collected at the Tormestorp magnetic observatory maintained by the Swedish Institute of Space Physics and at magnetic observatories. We thank the national institutes that support them and INTERMAGNET for promoting high standards of magnetic observatory practice ([www.intermagnet.org](http://www.intermagnet.org)). Finally, we thank several colleagues that has provided valuable input to this work.

## References

- Amm, O., & Viljanen, A. (1999). Ionospheric disturbance magnetic field continuation from the ground to the ionosphere using spherical elementary current systems. *Earth Planets and Space*, 51(6), 431–440. <https://doi.org/10.1186/BF03352247>
- Baker, D. N. (2008). *Severe space weather events—understanding societal and economic impacts*. The National Academies Press, National Research Council of the National Academies. 1–144.
- Bolduc, L. (2002). GIC observations and studies in the Hydro-Québec power system. *Journal of Atmospheric and Solar-Terrestrial Physics*, 64(16), 1793–1802. [https://doi.org/10.1016/S1364-6826\(02\)00128-1](https://doi.org/10.1016/S1364-6826(02)00128-1)
- Boteler, D. (2001). Assessment of geomagnetic hazard to power systems in Canada. *Natural Hazards: Journal of the International Society for the Prevention and Mitigation of Natural Hazards*, 23(2), 101–120. Retrieved from <https://ideas.repec.org/a/spr/nathaz/v23y2001i2p101-120.html>
- Boteler, D. (2006). The super storms of august/september 1859 and their effects on the telegraph system. *Advances in Space Research*, 38(2), 159–172. (The Great Historical Geomagnetic Storm of 1859: A Modern Look). Retrieved from <http://www.sciencedirect.com/science/article/pii/S0273117706000214>
- Boteler, D. H. (2013). Space weather effects on power systems. In *Space weather* (pp. 347–352). American Geophysical Union (AGU). <https://doi.org/10.1029/GM125p0347>
- Carrington, R. C. (1859). *Description of a Singular Appearance Seen in the Sun on September 1, 1859* (Vol. 20, pp. 13–15). Monthly Notices of the Royal Astronomical Society.
- Chave, A. D., & Jones, A. G. (2012). *The magnetotelluric method: Theory and practice*. Cambridge University Press.
- Davidson, W. F. (1940). The Magnetic Storm of March 24, 1940-effects in the Power System (pp. 359–364). *Edison Electric Institute Bulletin*(July).
- Dimmock, A. P., Rosenqvist, L., Hall, J.-O., Viljanen, A., Yordanova, E., Honkonen, I., et al. (2019). The gic and geomagnetic response over fennoscandia to the 7–8 september 2017 geomagnetic storm. *Space Weather*, 17(7), 989–1010. <https://doi.org/10.1029/2018SW002132>
- Dimmock, A. P., Rosenqvist, L., Welling, D. T., Viljanen, A., Honkonen, I., Boynton, R. J., & Yordanova, E. (2020). On the regional variability of db/dt and its significance to gic. *Space Weather*, 18(8), e2020SW002497. Retrieved from <https://agupubs.onlinelibrary.wiley.com/doi/abs/10.1029/2020SW002497>
- Dimmock, A. P., Welling, D. T., Rosenqvist, L., Forsyth, C., Freeman, M. P., Rae, I. J., et al. (2021). Modeling the geomagnetic response to the september 2017 space weather event over fennoscandia using the space weather modeling framework: Studying the impacts of spatial resolution. *Space Weather*, 19(5), e2020SW002683. Retrieved from <https://agupubs.onlinelibrary.wiley.com/doi/abs/10.1029/2020SW002683>
- Divett, T., Ingham, M., Beggan, C. D., Richardson, G. S., Rodger, C. J., Thomson, A. W. P., & Dalzell, M. (2017). Modeling geoelectric fields and geomagnetically induced currents around New Zealand to explore GIC in the south island's electrical transmission network. *Space Weather*, 15(10), 1396–1412. <https://doi.org/10.1002/2017SW001697>
- Egbert, G. D., & Livelybrooks, D. W. (1996). Single station magnetotelluric impedance estimation: Coherence weighting and the regression m-estimate. *Geophysics*, 61(4), 964–970. <https://doi.org/10.1190/1.1444045>
- Engels, M., & Korja, T., & Bear Working Group. (2002). Multisheet modelling of the electrical conductivity structure in the Fennoscandian shield. *Earth Planets and Space*, 54(5), 559–573. <https://doi.org/10.1186/BF03353045>
- Gao, J., Smirnov, S., Smirnova, M., & Egbert, G. (2021). 3-d time-domain electromagnetic modeling based on multi-resolution grid with application to geomagnetically induced currents. *Physics of the Earth and Planetary Interiors*, 312, 106651. Retrieved from <https://www.sciencedirect.com/science/article/pii/S003192021000091>
- Gilbert, J. L. (2005). Modeling the effect of the ocean-land interface on induced electric fields during geomagnetic storms. *Space Weather*, 3(4). <https://doi.org/10.1029/2004SW000120>
- Haiducek, J. D., Welling, D. T., Morley, S. K., Ganushkina, N. Y., & Chu, X. (2020). Using multiple signatures to improve accuracy of substorm identification. *Journal of Geophysical Research: Space Physics*, 125(4), e2019JA027559. Retrieved from <https://agupubs.onlinelibrary.wiley.com/doi/abs/10.1029/2019JA027559>
- Honkonen, I., Kuvshinov, A., Rastätter, L., & Pulkkinen, A. (2018). Predicting global ground geoelectric field with coupled geospace and three-dimensional geomagnetic induction models. *Space Weather*, 16(8), 1028–1041. Retrieved from <https://agupubs.onlinelibrary.wiley.com/doi/abs/10.1029/2018SW001859>
- Ivannikova, E., Kuvshinov, M., Kuvshinov, A., Rastätter, L., & Pulkkinen, A. (2018). Regional 3-d modeling of ground electromagnetic field due to realistic geomagnetic disturbances. *Space Weather*, 16(5), 476–500. <https://doi.org/10.1002/2017sw001793>
- Juusola, L., Vanhamäki, H., Viljanen, A., & Smirnov, M. (2020). Induced currents due to 3d ground conductivity play a major role in the interpretation of geomagnetic variations. *Annales Geophysicae*, 38(5), 983–998. Retrieved from <https://angeo.copernicus.org/articles/38/983/2020/>
- Kappenman, J. G. (2003). Storm sudden commencement events and the associated geomagnetically induced current risks to ground-based systems at low-latitude and midlatitude locations. *Space Weather*, 1(3). Retrieved from <https://agupubs.onlinelibrary.wiley.com/doi/abs/10.1029/2003SW000009>

- Kelbert, A. (2019). DecemberThe role of global/regional earth conductivity models in natural geomagnetic hazard mitigation. *Surveys in Geophysics*, 41(1), 115–166. <https://doi.org/10.1007/s10712-019-09579-z>
- Korja, T., Engels, M., Zhamaletdinov, A. A., Kovtun, A. A., Palshin, N. A., Smirnov, M. Y., & Vardaniants, I. L. (2002). Crustal conductivity in Fennoscandia - A compilation of a database on crustal conductance in the Fennoscandian Shield. *Earth Planets and Space*, 54, 535–558. <https://doi.org/10.1186/BF03353044>
- Ledo, J., Gabàs, A., & Marcuello, A. (2014). Static shift levelling using geomagnetic transfer functions. *Earth Planets and Space*, 54(5), 493–498. <https://doi.org/10.1186/BF03353040>
- Lettinen, M., & Pirjola, R. (1985). Current produced in earthed conductor networks by geomagnetically-induced electric fields. *Annales Geophysicae*, 3, 479–484.
- Love, J. J., Rigler, E. J., Pulkkinen, A., & Riley, P. (2015). On the lognormality of historical magnetic storm intensity statistics: Implications for extreme-event probabilities. *Geophysical Research Letters*, 42(16), 6544–6553. <https://doi.org/10.1002/2015GL064842>
- Lucas, G. M., Love, J. J., & Kelbert, A. (2018). Calculation of voltages in electric power transmission lines during historic geomagnetic storms: An investigation using realistic earth impedances. *Space Weather*, 16(2), 185–195. <https://doi.org/10.1002/2017SW001779>
- Marshall, R. A., Dalzell, M., Waters, C. L., Goldthorpe, P., & Smith, E. A. (2012). Geomagnetically induced currents in the New Zealand power network. *Space Weather*, 10(8). Retrieved from <https://agupubs.onlinelibrary.wiley.com/doi/abs/10.1029/2012SW000806>
- Marshall, R. A., Smith, E. A., Francis, M. J., Waters, C. L., & Sciffer, M. D. (2011). A preliminary risk assessment of the Australian region power network to space weather. *Space Weather*, 9(10). Retrieved from <https://agupubs.onlinelibrary.wiley.com/doi/abs/10.1029/2011SW000685>
- Ngwira, C. M., Pulkkinen, A., Leila Mays, M., Kuznetsova, M. M., Galvin, A. B., Simunac, K., et al. (2013). Simulation of the 23 July 2012 extreme space weather event: What if this extremely rare cme was earth directed? *Space Weather*, 11(12), 671–679. <https://doi.org/10.1002/2013SW000990>
- Ngwira, C. M., Pulkkinen, A. A., Bernabeu, E., Eichner, J., Viljanen, A., & Crowley, G. (2015). Characteristics of extreme geoelectric fields and their possible causes: Localized peak enhancements. *Geophysical Research Letters*, 42, 6916–6921. <https://doi.org/10.1002/2015GL065061>
- Ngwira, C. M., Sibeck, D., Silveira Marcos, V. D., Georgiou, M., Weygand, J. M., Nishimura, Y., & Hampton, D. (2018). A study of intense local db/dt variations during two geomagnetic storms. *Space Weather*, 16(6), 676–693. <https://doi.org/10.1029/2018SW001911>
- Oyedokun, D. T. O., Heyns, M. J., Cilliers, P. J., & Gaunt, C. T. (2019). Frequency components of geomagnetically induced currents for power system modelling. *arXiv e-prints*, arXiv:1912.09367.
- Pirjola, R. (2013). Practical model applicable to investigating the coast effect on the geoelectric field in connection with studies of geomagnetically induced currents. *Advances in Applied Physics*, 1, 9–28. <https://doi.org/10.12988/aap.2013.13002>
- Pulkkinen, A. (2003). *Geomagnetic induction during highly disturbed space weather conditions: Studies of ground effects*. PhD thesis. University of Helsinki.
- Pulkkinen, A., Bernabeu, E., Thomson, A., Viljanen, A., Pirjola, R., Boteler, D., et al. (2017). Geomagnetically induced currents: Science, engineering, and applications readiness. *Space Weather*, 15(7), 828–856. <https://doi.org/10.1002/2016SW001501>
- Pulkkinen, A., Hesse, M., Habib, S., Van der Zel, L., Damsky, B., Policelli, F., et al. (2010). Solar shield: Forecasting and mitigating space weather effects on high-voltage power transmission systems. *Natural Hazards*, 53(2), 333–345. <https://doi.org/10.1007/s11069-009-9432-x>
- Pulkkinen, A., Lindahl, S., Viljanen, A., & Pirjola, R. (2005). Geomagnetic storm of 29–31 October 2003: Geomagnetically induced currents and their relation to problems in the Swedish high-voltage power transmission system. *Space Weather*, 3(8). Retrieved from <https://agupubs.onlinelibrary.wiley.com/doi/abs/10.1029/2004SW000123>
- Pulkkinen, A., Pirjola, R., & Viljanen, A. (2008). Statistics of extreme geomagnetically induced current events. *Space Weather*, 6(7). Retrieved from <https://agupubs.onlinelibrary.wiley.com/doi/abs/10.1029/2008SW000388>
- Püthe, C., & Kuvshinov, A. (2013). September)Towards quantitative assessment of the hazard from space weatherGlobal 3-D modellings of the electric field induced by a realistic geomagnetic storm. *Earth Planets and Space*, 65, 1017–1025. <https://doi.org/10.5047/eps.2013.03.003>
- Rosenqvist, L., & Hall, J. O. (2019). Regional 3-d modeling and verification of geomagnetically induced currents in Sweden. *Space Weather*, 17(1), 27–36. Retrieved from <https://agupubs.onlinelibrary.wiley.com/doi/abs/10.1029/2018SW002084>
- Rosenqvist, L., Opgenoorth, H., Buchert, S., McCrea, I., Amm, O., & Lathuillere, C. (2005). Extreme solar-terrestrial events of October 2003: High-latitude and cluster observations of the large geomagnetic disturbances on 30 October. *Journal of Geophysical Research*, 110. <https://doi.org/10.1029/2004JA010927>
- Schrijver, C. J., & Beer, J. (2014). Space weather from explosions on the sun: How bad could it be? *Eos. Transactions - American Geophysical Union*, 95(24), 201–202. Retrieved from <https://agupubs.onlinelibrary.wiley.com/doi/abs/10.1002/2014EO240001>
- Smirnov, M. Y. (2003). Magnetotelluric data processing with a robust statistical procedure having a high breakdown point. *Geophysical Journal International*, 152(1), 1–7. <https://doi.org/10.1046/j.1365-246X.2003.01733.x>
- Svenska, K. (2011). *Skydd mot geomagnetiska stormar - Elektromagnetisk påverkan på kraftnätet*. (Tech. Rep.). Svenska kraftnät.
- Torta, J. M., Marcuello, A., Campaña, J., Marsal, S., Queralt, P., & Ledo, J. (2017). Improving the modeling of geomagnetically induced currents in Spain. *Space Weather*, 15(5), 691–703. <https://doi.org/10.1002/2017SW001628>
- Tóth, G., Meng, X., Gombosi, T. I., & Rastätter, L. (2014). Predicting the time derivative of local magnetic perturbations. *Journal of Geophysical Research: Space Physics*, 119(1), 310–321. <https://doi.org/10.1002/2013JA019456>
- Tozzi, R., De Michelis, P., Coco, I., & Giannattasio, F. (2019). A preliminary risk assessment of geomagnetically induced currents over the Italian territory. *Space Weather*, 17(1), 46–58. Retrieved from <https://agupubs.onlinelibrary.wiley.com/doi/abs/10.1029/2018SW002065>
- Tsurutani, B. T., & Lakhina, G. S. (2014). An extreme coronal mass ejection and consequences for the magnetosphere and earth. *Geophysical Research Letters*, 41(2), 287–292. Retrieved from <https://agupubs.onlinelibrary.wiley.com/doi/abs/10.1002/2013GL058825>
- Viljanen, A., Tanskanen, E., & Pulkkinen, A. (2006). Relation between substorm characteristics and rapid temporal variations of the ground magnetic field. *Annales Geophysicae*, 24. <https://doi.org/10.5194/angeo-24-725-2006>
- Welling, D. T., Love, J. J., Rigler, E. J., Oloveira, D. M., Komar, C. M., & Morley, S. K. (2020). *Numerical simulations of the geospace response to the 2 arrival of an idealized perfect interplanetary coronal 3 mass ejection*. submitted to Space Weather.
- Welling, D. T., Ngwira, C. M., Opgenoorth, H., Haiducek, J. D., Savani, N. P., Morley, S. K., et al. (2018). Recommendations for next-generation ground magnetic perturbation validation. *Space Weather*, 16(12), 1912–1920. Retrieved from <https://agupubs.onlinelibrary.wiley.com/doi/abs/10.1029/2018SW002064>
- Wik, M., Pirjola, R., Lundstedt, H., Viljanen, A., Wintoft, P., & Pulkkinen, A. (2009). Space weather events in July 1982 and October 2003 and the effects of geomagnetically induced currents on Swedish technical systems. *Annales Geophysicae*, 27(4), 1775–1787. <https://doi.org/10.5194/angeo-27-1775-2009>
- Zhang, J. J., Wang, C., Sun, T. R., Liu, C. M., & Wang, K. R. (2015). Gic due to storm sudden commencement in low-latitude high-voltage power network in China: Observation and simulation. *Space Weather*, 13(10), 643–655. Retrieved from <https://agupubs.onlinelibrary.wiley.com/doi/abs/10.1002/2015SW001263>